CARBONATION DEGREE IN CEMENTITIOUS MATERIALS BASED ON NONDESTRUCTIVE TESTING

Qizhen SHEN[1], Gaoxiang LOU[2*]

For the non-destructive assessment of carbonation zones in cementitious materials, X-ray computed tomography (XCT) tests were conducted on specimens with water-to-binder ratios of 0.35 and 0.53. The results of the gray level distribution revealed the presence of three distinct carbonation zones after the carbonation process: the fully carbonated zone, the partially carbonated zone, and the noncarbonated zone. An increase in the water-to-binder ratio corresponded to an expansion of both fully carbonated and partially carbonated zones. In comparison to specimens of pure cement paste, those incorporating supplementary cementitious materials (SCM) exhibited an enlarged partially carbonated zone, significantly impacting the distribution of carbonation zones. The findings demonstrate that the XCT method accurately detects the degree of carbonation, offering a novel perspective for assessing the carbonation of cementitious materials.

Keywords: Carbonation; Cement/ cementitious materials; X-ray computed tomography

1. Introduction

The carbonation of concrete involves concurrent physical and chemical processes [1] and is influenced by various factors [2] such as cement types, blended additives, carbon dioxide concentration, relative humidity, and more.

In the realm of cementitious material research, X-ray computed tomography (XCT) has been applied to investigate cement hydration processes, crack development, fracture processes [3-4], sulfate attack [5], interfacial transition zone (ITZ) [6], calcium leaching [7-8], pore structure, and tortuosity analysis [9]. XCT proves to be an outstanding non-invasive and nondestructive method for acquiring microstructure information on cementitious materials without necessitating prior specimen preparation, including vacuum drying, cutting, drilling, resin impregnation, grinding, and polishing.

Nevertheless, the utilization of XCT in the study of carbonation processes is infrequent. Han et al. [10-12] investigated the progression of the carbonation front, spatial distribution of cracks, and parameters of pore structure in hardened cement paste using XCT. In a previous work [13], the carbonation levels at different

[1] College of Civil Engineering, Ludong University, Yantai, Shandong, 264025, China
[2] College of Transportation, Ludong University, Yantai, Shandong, 264025, China, * corresponding author, e-mail: 11381238@qq.com

time intervals were assessed based on the volume fraction of noncarbonated and carbonated regions. Additionally, the porosity and distribution of pore volume in macropores were examined at various stages of carbonation. Wang [14] and Hong et al. [15] conducted a comparative analysis of results obtained from thermogravimetry analysis (TGA), XCT, and the phenolphthalein test. They observed that the carbonation depth measured by XCT fell between those obtained through the phenolphthalein test and the TGA method, thereby confirming the reliability of XCT results.

Considering the heterogeneity of cementitious materials and the alterations in their components during carbonation, there is a discernible impact on the shape of the carbonation front [16]. While TGA is a commonly employed method for precisely analyzing carbonation zones in existing literature [17], the determination of carbonation degree through testing the content of calcium hydroxide (CH) and $CaCO_3$ in cement is accurate. However, for the inclusion of supplementary cementitious materials (SCMs), the differentiation of carbonation zones becomes relatively challenging using TGA due to the complex nature of carbonation. The incorporation of blast furnace slag (BFS) and fly ash (FA) in cementitious materials results in the production of calcium silicate hydrate (C-S-H) gel and calcium aluminium hydrate (C-A-H) gel, leading to an overlap in the decomposition temperatures of C-S-H, C-A-H, and CH. Consequently, accurate detection by TGA becomes difficult [18]. In comparison, the nondestructive XCT test outperforms the TGA test. The XCT test relies on the changes in gray levels caused by the density increase of specimens after carbonation. To eliminate the need for sample drilling, a nondestructive XCT test was conducted to investigate the carbonation of cement paste, FA-cement paste, and BFS-cement paste under identical carbonation conditions. This study also explores the influence of supplementary cementitious materials and water-to-binder ratio on the carbonation zones of cementitious materials.

2. Experimental

2.1 Materials and mixtures

The cement utilized in this investigation was P·I 52.5. Tables 1 present the chemical and mineral compositions of the cement, fly ash (FA), and blast-furnace slag (BFS). Composition details of the paste are outlined in Table 2. As per project specifications (No. ZR2020QE250), the proportions of FA and BFS were set at 30% and 50%, respectively.

Table 1

Chemical composition of the cement, FA and BFS used (all values are in mass%)

	CaO	SiO_2	Al_2O_3	Fe_2O_3	MgO	K_2O	MnO	TiO_2	SO_3	Na_2O	P_2O_5	Others
P·I	64.69	21.61	4.32	3.10	1.30	0.82	0.18	0.27	2.60	0.18	0.10	0.83
FA	7.14	55.65	26.11	5.54	-	1.50	-	-	1.45	-	-	2.61
BFS	34.54	34.86	16.97	1.12	6.90	0.45	-	-	1.65	-		0.46

Table 2

Mix proportion of the binder paste

Water binder ratio	water (kg/m^3)	Cement(kg/m^3)	FA (kg/m^3)	BFS (kg/m^3)	Super plasticizer (%)
0.53	622	1179	0	0	0
		825	354	0	
		590	0	590	
0.35	514	1468	0	0	0.6
		1028	440	0	
		734	0	734	

2.2 Specimens and curing

Paste specimens of dimensions (40×40×160 mm) with water-to-binder (W/B) ratios of 0.35 and 0.53 were cast. The cement paste specimens were cured at 20 °C and 70% relative humidity (RH) for 24 hours, demolded, and subsequently placed in a curing room at (20±3) °C and 90% RH for 28 days. Specimens containing FA and BFS underwent a 90-day curing process. Post-curing, the specimens were subjected to a drying oven at 50 °C for 48 hours. After drying, the top and molding faces were sealed with paraffin, leaving the opposing parallel faces accessible for carbonation. Finally, the sealed specimens were introduced into a carbonation chamber with (20±2) % carbon dioxide, (70±5) % RH, and (20±2) °C.

2.3 Principle of XCT testing technology

XCT, a 3D imaging technique, reconstructs the X-ray absorption map of an object using a series of radiographic images. Fig.1 illustrates the principle of the CT system employed in this study. In XCT, a detector gauges the intensity of a known unidirectional X-ray beam after absorption by the material for various irradiation directions (θ), known as projections [19]. According to Beer-Lambert's law, the resulting intensity (I) on each pixel of the detector is expressed by Zhang [20]:

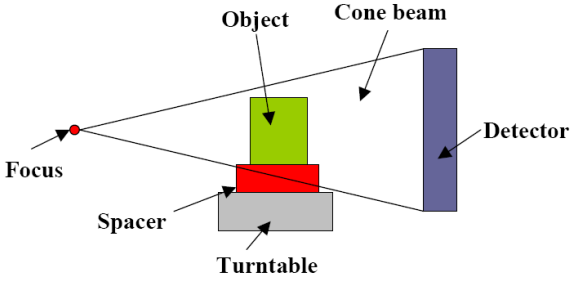

Fig. 1 Sketch map of XCT scanning principle

$$I = I_0 exp(-\int_L \mu_n dx) \quad (1)$$

where I_0 is the beam intensity before the sample, μ represents a large number of angles, and x is the thickness of material. The projection-slice theorem ensures the reconstruction of the 3D map of μ with adequate specimen sampling. The attenuation coefficient depends primarily on the density, thickness, and chemical composition of the sample materials. In this study, in-situ visual examination of specimens was conducted using Precision System (YXLON, Germany). The XCT scan parameters are detailed in Table 3.

Table 3

XCT scan parameters and standard setting

Parameter	X-ray tube voltage	X-ray tube current	Detector type	Rotation angles	Density resolution	Detector elements number	Projections number	Pixels number	2D pixel size	3D voxel size
Standard setting	195 kV	0.41 mA	Y.XRD 0820	360 degree	0.3%	1024	1080	1024 × 1024	0.08^2 mm^2	0.08^3 mm^3

During the XCT test, continuous sample rotation allowed the collection of projections from multiple angles. The attenuation coefficient data were stored in matrix form for analysis using computer software. The weighted Feldkamp arithmetic and geometric compensation method were employed for 3D image reconstruction [21-22].

Gray values in the reconstructed images represent absorption rates and attenuation coefficients at corresponding object positions. These gray values are proportional to the X-ray attenuation coefficient, strongly correlated with specimen density. The reconstructed result is a gray-scaled volume model of the evaluated object volume, comprised of volume elements (voxels). Higher gray values indicate greater absorption rates (density) at corresponding object positions. In this paper, the grayscale distribution of 2D images determined the cementitious material's attenuation coefficient at different depths before and after carbonation, and the analysis of various carbonation zones was conducted.

3. Results and discussion

3.1 Influence of W/B on carbonation front

Strength represents the most discernible impact of the water-to-binder (W/B) ratio on cementitious materials. Essentially, W/B influences the microstructure and, consequently, the durability of the cementitious material. A high W/B ratio results in increased porosity of the cementitious material, facilitating

carbon dioxide diffusion during carbonation. The cementitious material presented low carbonation resistance capability.

XCT VG Studio MAX 2.2 software was employed to select 2D images of hardened cement paste with varying water-cement ratios (W/C), as depicted in Fig. 2 and Fig. 3. The line gray value distribution of hardened cement paste with different cement ratios before carbonation was analyzed. In the gray value distribution figures, high gray values correspond to high density at the respective object positions. A sharp decrease in gray value indicates the presence of a pore or crack. As illustrated in Fig. 2 and Fig. 3, the XCT images of cement paste exhibit homogeneity, with negligible discrepancies in gray values between the interior and exterior. Fig. 4 displays the XCT gray level distribution of cement paste after 28 days of carbonation. Images (a) and (c) represent the 0.35 W/C cement paste, while (b) and (d) represent the 0.53 W/C cement paste. Simultaneously, phenolphthalein spray results are shown in Fig. 4 (e) and Fig. 4 (f).

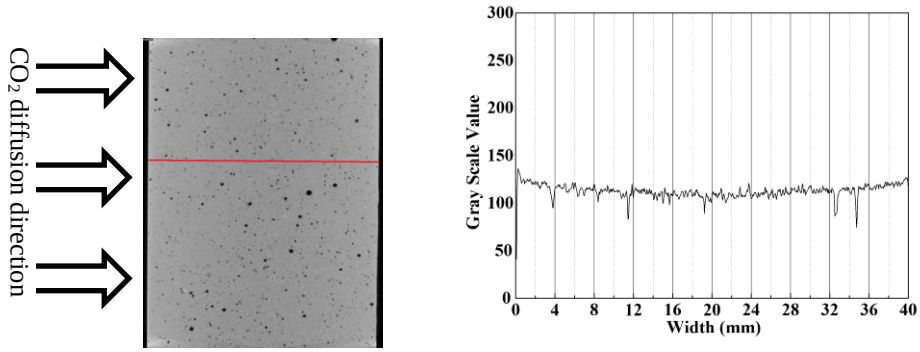

Fig.2. XCT image and gray values distribution of noncarbonated cement paste with 0.35W/C

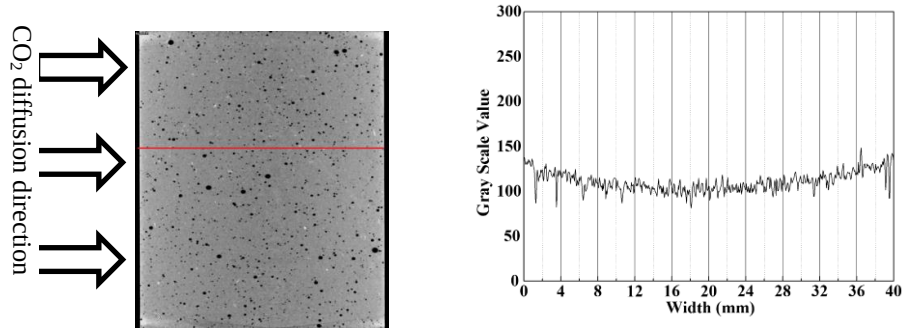

Fig.3. XCT image and gray values distribution of noncarbonated cement paste with 0.53W/C

As shown in Figs.2, 3, and 4, the generated high-density $CaCO_3$ increased the gray value of the specimens after carbonation. Fig. 4 (a) reveals a distinct carbonation front line in the 0.35 W/C cement specimen after 28 days, whereas no

such line is observed in the 0.53 W/C cement specimen. Phenolphthalein spray results (Fig. 4 e and f) corroborate the experimental results, confirming the carbonation depth determined by X-ray CT. The carbonation front line in the 0.35 W/C cement specimen is evident, albeit with a smaller carbonation depth. A higher W/C ratio within the same carbonation period results in larger porosity, enhancing carbon dioxide diffusion and, consequently, increasing carbonation depth

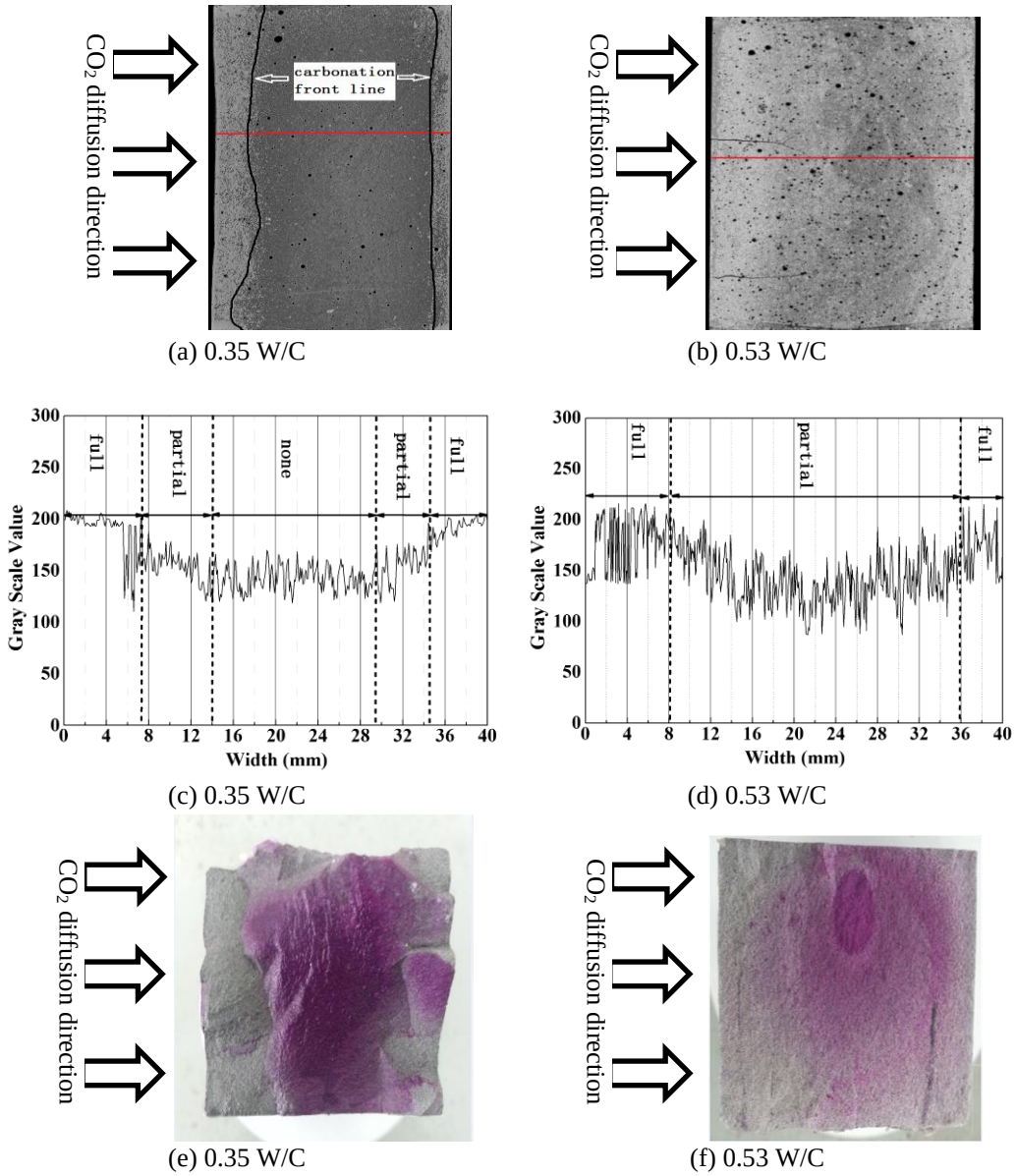

Fig. 4 The phenolphthalein test result and XCT gray level distribution of cement paste after carbonated for 28 days

Fig. 4(b) hereabove depicts significant cracks observed after carbonation in the 0.53 W/C cement specimen. The contraction stress induced by carbonation in the high W/C ratio specimen surpassed tensile strength, accelerating the carbonation process.

3.2 Availability verification of XCT

XCT can provide a non-invasive and nondestructive method to obtain reliable microstructure information on cementitious materials without any prior specimen preparation, such as vacuum drying, cutting, and drilling. Detection of the different carbonation zones in cementitious materials using XCT remains uncommon. To validate the efficacy of this method, thermogravimetric analysis (TGA) was conducted on 0.35 and 0.53 W/C cement pastes, with results depicted in Fig. 5.

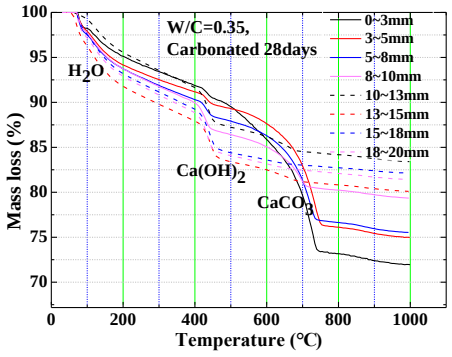

(a) 0.35W/C-TG

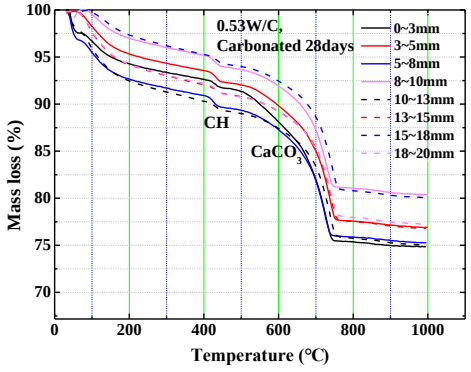

(d) 0.53W/C-TG

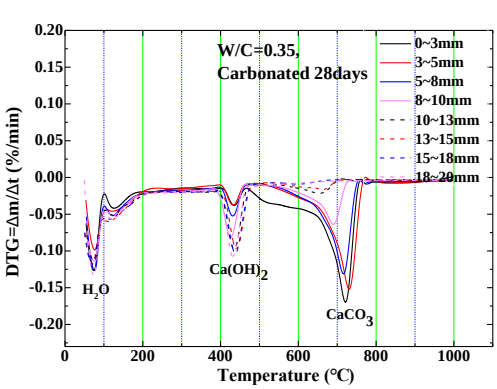

(b) 0.35W/C-DTG

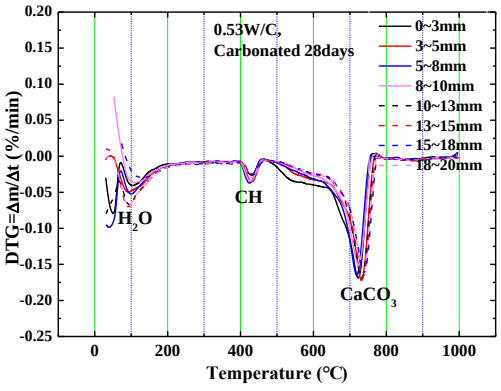

(e) 0.53W/C-DTG

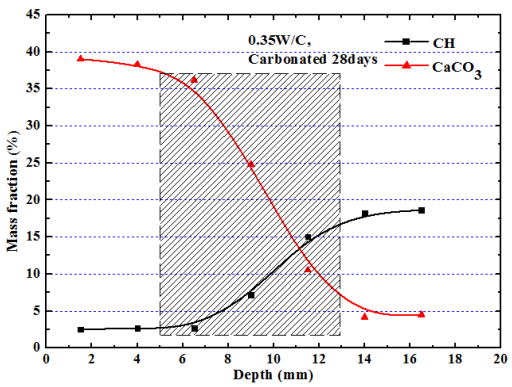

(c) Mass fraction of 0.35W/C-CH, $CaCO_3$

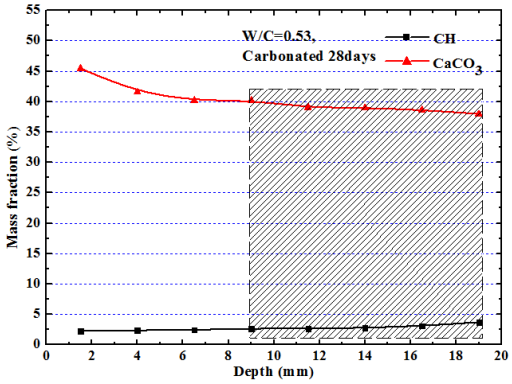

(f) Mass fraction of 0.53W/C-CH, $CaCO_3$

Fig. 5. TGA result of different carbonation depth and the mass fraction of CH and $CaCO_3$
Note: The shaded area represent the partial carbonated zone.

The carbonation depth of the 0.35 W/C cement paste, as determined by TGA, was approximately 13 mm. In the surface area to a depth of 5 mm, the mass fraction of calcium hydroxide (CH) was around 3.0%. Within a middle area approximately 8 mm wide, the mass fraction of CH increased from 3.0% to 18.2% before stabilizing. Based on CH mass fraction, the 0-5 mm depth represented the fully carbonated zone, followed by the partially carbonated zone at 5-13 mm depth and the noncarbonated zone beyond 13 mm. After 28 days of carbonation, the 0.53 W/C cement paste exhibited an almost unchanged solid phase, a CH mass fraction of around 2.5%, and the absence of a noncarbonated zone.

The distribution of the fully carbonated, partially carbonated, and noncarbonated zones is listed in Table 4. The results tested by TGA and XCT were consistent. The precision value of the solid phase from a certain layer can be measured by TGA, and the distribution of the solid phase can be nondestructively tested by XCT. The comprehensive test results of TGA and XCT showed that the carbonation front was not a sharp line but a transition zone, in which composition and density changed gradually.

Table 4

Distribution of the fully carbonated, partially carbonated, and noncarbonated zones (tested for a depth of 20 mm)

Test method	W/C	fully carbonated zone (*mm*)	partial carbonated zone (*mm*)	noncarbonated zone (*mm*)
TG	0.35	5	8	7
	0.53	9	11	0
X-CT	0.35	5	6	10
	0.53	8	12	0

3.3 Influence of SCMs on carbonation

In general, the cementitious properties of supplementary cementitious materials (SCM) arise from their pozzolanic effect. On one hand, the development of the pozzolanic effect primarily results from SCM reacting with the calcium hydroxide, a byproduct of cement hydration. Additionally, the consumption of calcium hydroxide accelerates cement hydration and densifies the cementitious material, thereby enhancing its resistance to carbonation. On the other hand, the consumption of calcium hydroxide reduces the alkaline content in the cementitious material, facilitating carbonation.

According to XCT principles, gray values are proportional to the X-ray attenuation coefficient, which strongly correlates with the density of the specimens. The bright areas in the image represent high density and correspond to large gray values. Following this principle, grayscale analysis of the XCT images was conducted, and the analysis results are presented in Fig. 6. High-density calcium carbonate generated in the surface layer resulted in larger gray values than those of the noncarbonated zone. The grayscale analysis revealed three distinct carbonation zones: the fully carbonated zone, the partially carbonated zone, and the noncarbonated zone. Table 5 outlines the distribution of each zone. Taking the specimen with W/B=0.35BFS (within 20 mm width) as an example, a relatively stable gray value was observed, representing the fully carbonated zone within the 0-4.5 mm depth range. The partially carbonated zone, with a gradual decrease in gray value, extended from 4.5 to 15 mm depth, while the noncarbonated zone within the 15-20 mm depth exhibited the smallest gray value and stability.

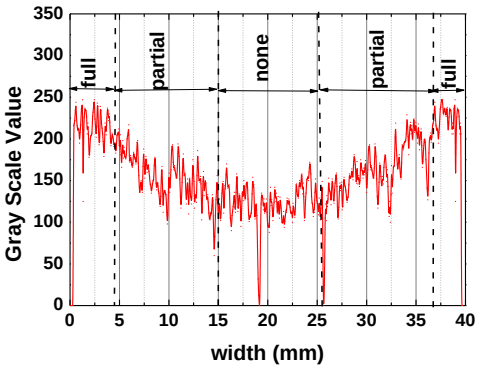

(a) W/B=0.35 BFS

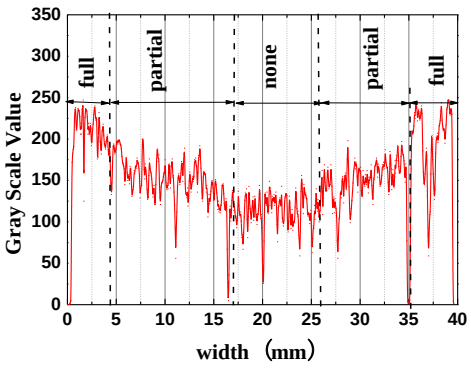

(b) W/B=0.35 FA

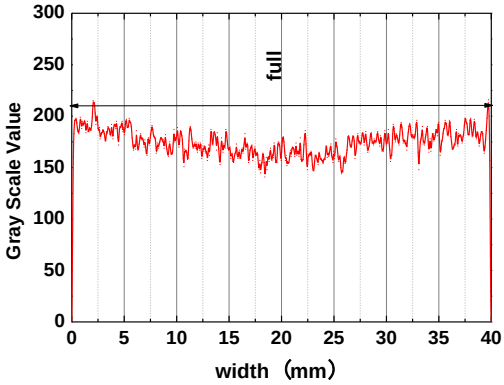

(c) W/B=0.53 BFS

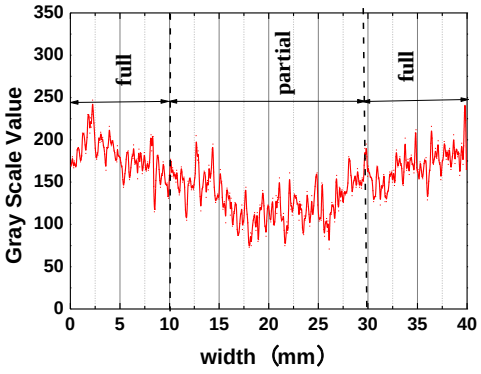

(d) W/B=0.53 FA

Fig. 6 The XCT gray level distribution of cement paste with SCM

Table 5

Distribution of the three carbonation zones tested by XCT/mm

specimens	fully carbonated zone	partially carbonated zone	noncarbonated zone
W/B=0.35 B	0-4.5	4.5-15	15-20
W/B=0.35 F	0-4.5	4.5-17	17-20
W/B=0.35P	0-5	5-11	11-20
W/B=0.53B	0-20	0	0
W/B=0.53 F	0-10	10-20	0
W/B=0.53P	0-8	8-20	0

In the comparison of cementitious paste with a water-binder ratio (W/B) of 0.35, SCMs demonstrated almost no effect on the size of the fully carbonated zone but exerted a discernible influence on the partially carbonated zone. Specimens mixed with SCM exhibited a larger size of the partially carbonated zone compared to that of the pure cement paste. Blended cement specimens, subjected to prolonged curing times, displayed increased density, with mineral admixture hydration yielding abundant low Ca/Si ratio C-S-H gels [23]. Glasser [24] highlighted that the surface of C-S-H gel with a high Ca/Si ratio is positively charged. As the Ca/Si ratio decreases, the surface of C-S-H gel loses its charge and is only governed by Van der Waals force. Lower Ca/Si ratio gels are more prone to adsorbing alkali metal ions, as demonstrated by Hong and Glasser [25], who proved that C-S-H gel with Ca/Si = 0.85-1.2 is more likely to attract alkali metal ions. In the pore solution, observations revealed the presence of not only calcium ions but also potassium and sodium ions. The solubility of calcium ions sharply decreased with an increase in alkali ions. Diamond [26] pointed out that, after a few months, the number of calcium ions in the pore solution became extremely small due to calcium hydroxide being enveloped with a layer of impermeable silicon film, separating calcium

hydroxide from the pore solution. Building upon these observations, Houst formulated the carbonation equation as follows [27]:

$$CO_2 + 2NaOH \rightarrow Na_2CO_3 + H_2O \quad (2)$$

$$Na_2CO_3 + Ca(OH)_2 \rightarrow CaCO_3\downarrow + 2NaOH \quad (3)$$

$$2Na_2CO_3 + 3CaO \cdot SiO_2 \cdot 4H_2O \rightarrow 3CaCO_3\downarrow + 2SiO_2 + 6NaOH + H_2O \quad (4)$$

According to Equation 4, alkali metal ions during carbonation behave similarly to catalysts. When the content of alkali metal ions in the solution decreases, the rate of carbonation markedly decreases. According to the research of Glasser [24], C-S-H gel with a low Ca/Si ratio more easily adsorbs alkali metal ions, indicating that the pore solution of blended cement specimens with a low alkali metal ion concentration slows down carbonation. Thus, despite being lower in blended cement specimens compared to that of pure cement paste, alkali content exerts little effect on the size of the fully carbonated zone.

From the carbonation results of the specimens with W/B=0.53 (pure cement paste samples, cement paste with FA, and cement paste with BFS), the size and distribution of the partial carbonation zone were evidently influenced by the SCM compared to that of the W/B = 0.35 group. The W/B = 0.53 specimens had a high W/B ratio, leading to the formation of large cracks caused by the shrinkage of carbonation. The XCT images clearly revealed that these cracks accelerated carbonation. Meanwhile, the specimens with SCM contained a low content of calcium hydroxide and a high content of C-S-H gel. Several studies [28] have shown that the carbonation of C-S-H generates silica gel, producing a condensation effect that induces shrinkage and cracking, reduces the volume, and deteriorates the pore structure.

For low W/B, SCM minimally impacted the size of the fully carbonated zone but significantly affected the partial carbonation zone in specimens with 30% FA or 50% BFS. In the case of high W/B, the carbonation depth of SCM-containing specimens was notably larger than that of pure cement paste samples. Small W/B resulted in smaller fully carbonated and partially carbonated zones.

4. Conclusions

TGA and XCT methods were employed to determine carbonation depth. The results demonstrated that the XCT nondestructive test accurately determined carbonation depth, validated by TGA testing. For cement-based materials mixed with SCM, TGA faced challenges in accurately testing carbonation depth due to the complexity of carbonation products. XCT effectively addressed this issue, providing a nondestructive testing scheme for accurately measuring carbonation depth in cement-based materials mixed with SCM in engineering.

For specimens with larger W/B ratios, carbonation depth was greater, accompanied by more significant cracks observed in XCT images. In samples with a low water-to-binder ratio (W/B=0.35), the addition of SCM had minimal effect on the size of the fully carbonated zone but significantly influenced the size of the partial carbonation zone, which was larger than that of pure cement paste samples. In samples with a high water-to-binder ratio (W/B=0.53), the addition of SCM notably impacted the size of both the fully carbonated and partial carbonation zones.

Acknowledgment

The authors acknowledge the financial support from the Shandong Provincial Natural Science Foundation (No. ZR2020QE250).

REFERENCES

[1] *Joshi, S., Ahn, Y.H., Goyal, S., Reddy, M. S.,* Performance of bacterial mediated mineralization in concrete under carbonation and chloride induced corrosion. Journal of Building Engineering, 2023,106234. https://doi.org/10.1016/j.jobe.2023.106234

[2] *Al-Ameeri, A. S., Rafiq, M. I., Tsioulou, O., & Rybdylova, O.,* Impact of climate change on the carbonation in concrete due to carbon dioxide ingress: Experimental investigation and modelling. Journal of Building Engineering, 2021, 44: 102594. https://doi.org/10.1016/j.jobe.2021.102594

[3] *Shakoorioskooie, M., Griffa, M., Leemann, A., Zboray, R., & Lura, P.,* Alkali-silica reaction products and cracks: X-ray micro-tomography-based analysis of their spatial-temporal evolution at a mesoscale. Cement and Concrete Research, 2021, 150: 106593. https://doi.org/10.1016/j.cemconres.2021.106593

[4] *Andrade, C., Saucedo, L., Rebolledo, N., Cabeza, S., & Meinel, D.,* X-Ray computed tomography and traditional analysis of a capillary absorption test in cement pastes. Cement and Concrete Composites, 2020, 113: 103634. https://doi.org/10.1016/j.cemconcomp.2020.103634

[5] *Badgujar, S., & Dwivedi, A. K.,* Microstructural analysis of Self-Compacting Concrete– A review. Materials Today: Proceedings, 2022, 65(Part 2): 1250-1259. https://doi.org/10.1016/j.matpr.2022.04.185

[6] *Robuschi, S., Tengattini, A., Dijkstra, J., Fernandez, I., & Lundgren, K.,* A closer look at corrosion of steel reinforcement bars in concrete using 3D neutron and X-ray computed tomography. Cement and Concrete Research, 2021, 144:106439. https://doi.org/10.1016/j.cemconres.2021.106439

[7] *Sugiyama, T., & Promentilla, M. A. B.,* Advancing Concrete Durability Research through X-ray Computed Tomography. Journal of Advanced Concrete Technology, 2021, 19(6):730-755. https://doi.org/10.3151/jact.19.730

[8] *Brisard, S., Serdar, M., & Monteiro, P. J.,* Multiscale X-ray tomography of cementitious materials: A review. Cement and Concrete Research, 2020, 128: 105824. https://doi.org/10.1016/j.cemconres.2019.105824

[9] *Shah, V., Mackechnie, J., & Scott, A.,* Determination of carbonation resistance of concrete through a combination of cement content and tortuosity. Journal of Building Engineering, 2022, 60: 105176. https://doi.org/10.1016/j.jobe.2022.105176

[10] H*an, J., Sun, W., Pan, G., Wang, C., & Rong, H.,* Application of X-ray Computed Tomography in Characterization Microstructure Changes of Cement Pastes in Carbonation

Process. Journal of Wuhan University of Technology (Materials Science Edition), 2012, 27: 358-363. https://doi.org/10.1007/s11595-012-0466-7

[11] *Han, J., Liang, Y., Sun, W., Liu, W., & Wang, S.*, Microstructure Modification of Carbonated Cement Paste with Six Kinds of Modern Microscopic Instruments. Journal of Materials in Civil Engineering, 2015, 27(10):04014262. https://doi.org/10.1061/(ASCE)MT.1943-5533.0001210

[12] *Han, J., Sun, W., & Pan, G.*, In situ dynamic XCT imaging of the microstructure evolution of cement mortar in accelerated carbonation reaction. Magazine of Concrete Research, 2012, 64(11):1025-1031. https://doi.org/10.1680/macr.11.00173

[13] *Han, J., Sun, W., & Pan, G.*, X-ray Microtomography of the Carbonation Front Shape Evolution of Cement Mortar and Modeling of Accelerated Carbonation Reaction. Journal of Wuhan University of Technology (Materials Science Edition), 2013,28:303-308. https://doi.org/10.1007/s11595-013-0683-8

[14] *Wang, Y.D.,* Investigation on Microstructure of Concrete under Carbonation[D]. Nanjing: Southeast University, 2012.

[15] *Hong, S., Jiang, R., Zheng, F., Fan, S., & Dong, B.,* Quantitative characterization of carbonation of cement-based materials using X-ray imaging. Cement and Concrete Composites, 2022,134: 104794. https://doi.org/10.1016/j.cemconcomp.2022.104794

[16] *Han, J., Sun, W., & Pan, G.*, Nondestructive microstructure analysis of the carbonation evolution process in hardened binder paste containing blast-furnace slag by X-ray CT. Journal of Wuhan University of Technology (Materials Science Edition), 2013. 28: 955-962. https://doi.org/10.1007/s11595-013-0800-8

[17] *Shen, Q., Pan, G., & Bao, B.*, Influence of CSH carbonation on the porosity of cement paste. Magazine of Concrete Research, 2016, 68(10):504-514. https://doi.org/10.1680/jmacr.15.00286

[18] *Bernal, S. A., Provis, J. L., Walkley, B., San Nicolas, R., Gehman, J. D., Brice, D. G., van Deventer, J. S.*, Gel nanostructure in alkali-activated binders based on slag and fly ash, and effects of accelerated carbonation. Cement and Concrete Research, 2013, 53: 127-144. https://doi.org/10.1016/j.cemconres.2013.06.007

[19] *Zhang, M., He, Y., Ye, G., Lange, D. A., & Van Breugel, K.,* Computational investigation on mass diffusivity in Portland cement paste based on X-ray computed microtomography (μCT) image. Construction and Building Materials, 2012, 27 (1): 472-481. https://doi.org/10.1016/j.conbuildmat.2011.07.017

[20] *Zhang, Z.Z.,* Industrial CT technology and principle [M]. Beijing: Science Press, 2009.

[21] *Balázs, G. L., Lublóy, É., & Földes, T.*, Evaluation of Concrete Elements with X-Ray Computed Tomography. Journal of Materials in Civil Engineering, 2018, 30(9): 06018010. https://doi.org/10.1061/(ASCE)MT.1943-5533.0002389

[22] *Isgor, O. B., & Razaqpur, A. G.,* Finite element modeling of coupled heat transfer, moisture transport and carbonation processes in concrete structures. Cement and Concrete Composites, 2004, 26 (1):57-73. https://doi.org/10.1016/S0958-9465(02)00125-7

[23] *Taylor, H. F., Mohan, K., & Moir, G. K.,* Analytical study of pure and extended Portland cement pastes: II, fly ash- and slag-cement pastes. Journal of the American Ceramic Society, 1985, 68(12):685-690. https://doi.org/10.1111/j.1151-2916.1985.tb10125.x

[24] *Glasser, F. P., & Marr, J.,* Alkali binding potential of OPC and blended cements. Cemento, 1985, 82(2):85-94.

[25] *Hong, S. Y., & Glasser, F. P.,* Alkali binding in cement pastes: Part I. The C-S-H phase. Cement and Concrete Research, 1999, 29(12):1893-1903. https://doi.org/10.1016/S0008-8846(99)00187-8

[26] *Diamond, S.,* Long-term status of calcium hydroxide saturation of pore solution in hardened cements. Cement and Concrete Research, 1975, 5(6):607-616. https://doi.org/10.1016/0008-

8846(75)90061-7

[27] *Houst, Y. F., & Wittmann, F. H.,* Depth profiles of carbonates formed during natural carbonation. Cement and Concrete Research, 2002, 32(12):1923-1930. https://doi.org/10.1016/S0008-8846(02)00908-0

[28] *Kropp, T. A. B. J., & Hilsdorf, H. K.,* The formation of silica gel during carbonation of cementitious systems containing slag cements. Special Publication, 1989, 114: 1413-1428. DOI: 10.14359/1817